Effect of Sn for the dislocation-free SiSn nanostructure formation on the vapor-liquid-crystal mechanism

Cite as: AIP Advances 10, 015309 (2020); doi: 10.1063/1.5139936
Submitted: 23 November 2019 • Accepted: 17 December 2019 •
Published Online: 7 January 2020

Vyacheslav Timofeev,[1,a)] Vladimir Mashanov,[1] Alexander Nikiforov,[1,2] Ilya Skvortsov,[1,3] Tatyana Gavrilova,[1] Dmitry Gulyaev,[1] Anton Gutakovskii,[1,3] and Igor Chetyrin[4]

AFFILIATIONS

[1] Rzhanov Institute of Semiconductor Physics SB RAS, 13 Lavrentyev Avenue, Novosibirsk 630090, Russia
[2] National Research Tomsk State University, 36 Lenin Avenue, Tomsk 634050, Russia
[3] Novosibirsk State University, 1 Pirogov Str., Novosibirsk 630090, Russia
[4] Boreskov Institute of Catalysis SB RAS, 5 Lavrentyev Avenue, Novosibirsk 630090, Russia

[a)] **Author to whom correspondence should be addressed:** Vyacheslav.t@isp.nsc.ru

ABSTRACT

Structures with tin-rich island arrays on silicon pedestals were obtained by molecular beam epitaxy using Sn as a catalyst for the growth of nanostructures. A tin island array was used further to study the growth of nanostructures in the process of Si deposition on the surface with Sn islands. It was established that, during the growth on the vapor-liquid-crystal mechanism, tin-rich islands are formed on faceted pedestals. A nanostructured cellular surface was formed between the islands on pedestals. The analysis of the elemental composition of the obtained nanostructures was performed by the methods of energy dispersive X-ray spectroscopy and photoelectron spectroscopy. It is shown that tin-rich islands can contain up to 90% tin, whereas the pedestal consists of silicon. The transmission electron microscopy data demonstrated a distinct crystal structure of tin-rich islands and silicon pedestals, as well as the absence of dislocations in the structures with island arrays on the faceted pedestals. The facet tilt angle is 19° and corresponds to the (311) plane. The photoluminescence signal was observed with a photoluminescence maximum near the wavelength of 1.55 μm.

© 2020 Author(s). All article content, except where otherwise noted, is licensed under a Creative Commons Attribution (CC BY) license (http://creativecommons.org/licenses/by/4.0/). https://doi.org/10.1063/1.5139936

I. INTRODUCTION

Ge-Si-Sn materials have attracted great attention of scientists due to the possibility of obtaining a direct bandgap material by adding Sn to the GeSi matrix. In recent years, the direct bandgap GeSn material has been demonstrated,[1] and photodetectors,[2] LEDs,[3,4] and lasers[5–7] based on Ge-Si-Sn materials have been presented. Besides, the prospects of creating a direct bandgap material are found in the adjusting of electrophysical properties by including deformations and changing the bandgap. The implementation of type I heterostructures allows controlling the charge carrier limitation.[8] Such structures will find the application in transistors with high carrier mobility, LEDs, quantum well lasers, and also solar cells. The reduced dimensional systems based on the Ge-Si-Sn materials, such as quantum wires and quantum dots, demonstrate new perspectives and properties that are not observed in the bulk material.[9]

Recent advances in the field of the device development using nanowires cover the fields from nanoelectronics (field effect transistors) up to superconductivity.[10–12] The direct bandgap emitting structures, which operate in the mid-IR range and contain a GeSn nanowire array with the high Sn content, were obtained.[13] The next promising candidate exhibiting quantum-size effects is quantum dots. New optical and electronic properties arise due to the limitation of charge carriers in all three motion directions. Since the huge interest is observed relative to the quantum dots in the field of the display creation, investigations are mainly aimed at the search of approaches and materials with improved luminescent

© Author(s) 2020

properties.[14] Recently, the photoluminescence in the visible range has been demonstrated in the contributions,[15,16] which are devoted to the GeSn quantum dots. By changing the composition and size of quantum dots, one can control the photoluminescence spectrum. The orange-red photoluminescence was observed for the quantum dots in the size range from 1 to 3 nm. The tin content ranged from 1.8% to 23.6%. Despite the fact that quantum dots containing Cd are currently used in the manufacture of displays, alternative materials are being sought. The quantum dots based on group IV materials (Ge, Si, and Sn) can become nontoxic, stable, and cost-effective.

The main objective of this contribution was to study the SiSn nanoisland growth on a silicon pedestal, using Sn as a growth catalyst by using the molecular beam epitaxy method. The SiSn island formation occurred on the vapor-liquid-crystal (VLC) mechanism. In addition to the array of islands on pedestals, a nanostructured cellular silicon surface, which can be promising for creating the dense quantum dot array based on Ge-Si-Sn materials, was observed.

II. EXPERIMENTAL DETAILS

The Sn islands and Sn-rich islands with Si pedestals on the Si(100) substrate were obtained by the molecular-beam epitaxy (MBE) technique at ultrahigh vacuum conditions of 10^{-7}–10^{-8} Pa. The MBE chamber is equipped with the electron beam evaporator for Si and the Knudsen effusion cell for Sn. The Sn and Si layer growth rates were varied from 0.012 to 0.02 nm/s and from 0.53 to 1 nm/s, respectively. The growth and annealing temperatures were changed in the range of 300–600 °C. The Sn film on the Si surface was formed on the first step and then annealed to create the Sn island arrays, which were applied as nanoobject growth catalysts. The further Si deposition on this surface with the Sn islands resulted in the appearance of Sn-rich islands with Si pedestals. The main method of the morphology and surface structure control was reflection of high energy electron diffraction (RHEED). The transition from the two-dimensional to three-dimensional film (2D–3D transition) during the Sn island growth was observed in the RHEED patterns. The appearance of the Sn-rich islands with Si pedestals was also monitored on the RHEED patterns. The film morphology including the Sn islands and Sn-rich islands with pedestals was analyzed by using a scanning electron microscope (SEM) (Hitachi SU8220) and a scanning tunneling microscope (STM) (Omicron-Riber). The SEM system allows carrying out the element analysis of the grown samples since it additionally includes the EDX (Energy-dispersive X-Ray spectroscopy) Bruker detectors. The XFlash 5060F QUAD detector included in the SEM equipment was used for the analysis of the X-Ray spectrum emission energy of the structures obtained by the MBE technique. The morphology and atomic structure of the SiSn islands on the Si substrate were investigated by means of high-resolution electron microscopy (HREM) of cross section (110) using a Titan 80–300 (FEI) transmission electron microscope with a point to point resolution of 0.08 nm, operated at 300 kV. The analysis of the material chemical state both in its initial state and after the exposition with Ar^+ ions was carried out using the SPECS X-Ray photoelectron spectrometer (Germany). The spectrometer consists of three main vacuum chambers: a loading chamber, a preparation chamber, and an analyzer chamber equipped with manipulators for the sample transfer. The base pressure in the preparation chamber is 5×10^{-9} mbar and is maintained by a turbomolecular pump. The analyzer chamber is meant to record photoelectron spectra and is equipped with the hemispherical analyzer PHOIBOS-150-MCD-9, the FOCUS-500 X-Ray monochromator, and the XR-50M X-Ray source with the double Al/Ag anode. The base pressure in the analyzer chamber is about 5×10^{-10} mbar. In this work, the characteristic monochromatic radiation $AlK\alpha_{1,2}$ ($h\nu$ = 1486.74 eV, 200 W) was used to excite the spectra. The preparation chamber of this spectrometer is equipped with an argon gun, which allows the soft etching of the investigated sample surface in order to remove surface impurities and oxide films. The sample optical properties were studied by photoluminescence (PL) spectroscopy. To excite the photoluminescence, a YAG:Nd laser with the wavelength of 527 nm and the maximum power of 170 mW was used. The photoluminescence was registered by the spectrometer based on the double diffraction monochromator equipped with the Ge detector (the sensitivity range of 0.8–1.7 μm). The PL measurements were carried out at the nitrogen (77 K) and room (300 K) temperatures.

III. RESULTS AND DISCUSSION

The SiSn nanostructure growth was studied at the Si deposition on the surface with a Sn island array. A series of structures with different thicknesses in the range from 0 to 20 nm was obtained. At the first step, the Sn film was deposited on the Si surface either at room temperature or at 100 °C. The surface morphology was controlled on the RHEED pattern. The polycrystalline Sn film was formed, and it was confirmed by the presence of rings on the RHEED pattern [Fig. 1(a)]. Then, the Sn films were annealed. The annealing process was also observed on the RHEED patterns. During the annealing, the disappearance of the rings corresponding to the polycrystalline film took place, and the transition from the polycrystalline film to the film with the Sn island array was observed. The occurrence of 3D reflexes was controlled on the RHEED pattern [Fig. 1(b)]. The broadening of reflexes and the increase of their brightness were observed during the Si deposition on the surface with a Sn island array. It is associated with an increase in the island size [Fig. 1(c)]. The initial Sn island array is shown in the scanning electron microscopy (SEM) image in the secondary electrons [Fig. 2(a)]. The tilted surface sites

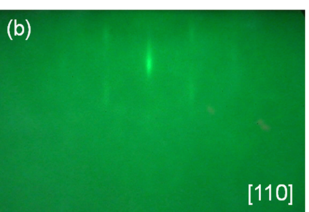

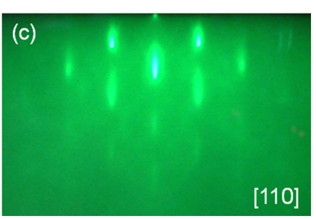

FIG. 1. (a) RHEED pattern from the polycrystalline film during the Sn deposition; (b) RHEED pattern from Sn islands after annealing; and (c) RHEED pattern from SiSn islands after the Si deposition on the Sn island array.

© Author(s) 2020

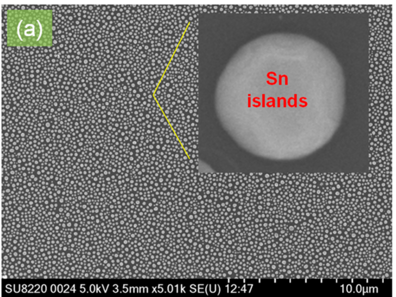

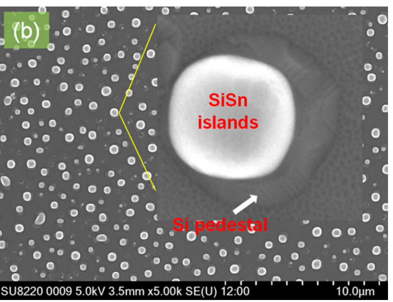

FIG. 2. SEM sample surface images: (a) for the Sn island array after annealing the polycrystalline Sn film (the Sn island increased by a factor 40 as shown in the inset) and (b) for the SiSn island array with the Si pedestal obtained after the Si deposition over the Sn island array (the SiSn island increased by a factor 15 as shown in the inset).

in the SEM image of the secondary electrons look brighter, compared with the surface perpendicular to the primary incident beam. The increase in the secondary electron yield occurs near the acute edges and angles of the sample. It is connected with a possibility of the yield through several surfaces. Sn gives an additional contribution to the secondary electron emission as it has a more complicated electron configuration than that of Si. In the inset of Fig. 2(a) is the Sn island enlarged by a factor of 40. The SEM surface image with the island array, obtained during the Si deposition over the film with a tin island array, is presented in Fig. 2(b). The distribution histograms for the number of islands on the base size and density for the Sn island arrays, also for the islands with a pedestal, are presented.[17] It is possible to see that the island is formed on the pedestal in the enlarge island image [inset of Fig. 2(b), enlarged by a factor of 15]. The pedestal is faceted by a distinct facet. One can identify the facet from the island array on the pedestal by using either the RHEED pattern or the TEM image. The RHEED pattern with the faces from the pedestals is shown in Fig. 3. The facet tilt angle equals 19°, and it corresponds to the facet (311). The same result is confirmed by the STEM (scanning transmission electron microscopy) data (Fig. 4). The pedestal-faceting planes are clearly seen in the STEM image. They also correspond to the facet (311). Besides, it is possible to conclude from the investigation results obtained by TEM that our structures do not have any dislocations (Fig. 5). There are no dislocations observed at the (tin-rich) island-Si border in the cross-sectional image. The island merging process leads to the appearance of faceted pits. The distinct faceting of the pits shaped as a reverse pyramid with the ⟨110⟩ type base rib direction can be observed in the SEM images (Fig. 6, Table I). The Sn deposition at the temperature of 300 °C is a considerable difference of the sample presented in Fig. 6 from the previous samples. The Sn island array was formed without using any additional annealing. The Sn islands self-organize

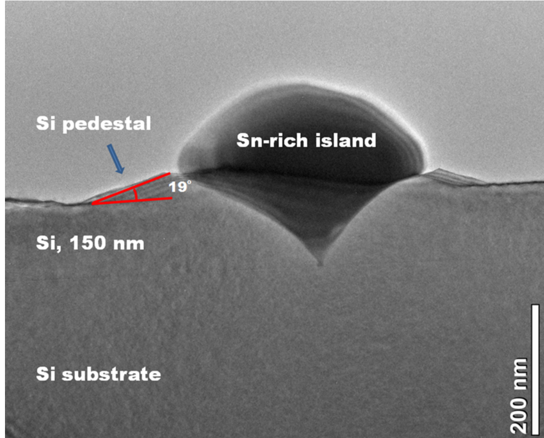

FIG. 4. Cross-sectional STEM image for one of the Sn-rich islands with the Si pedestal. The facet angle equals 19°.

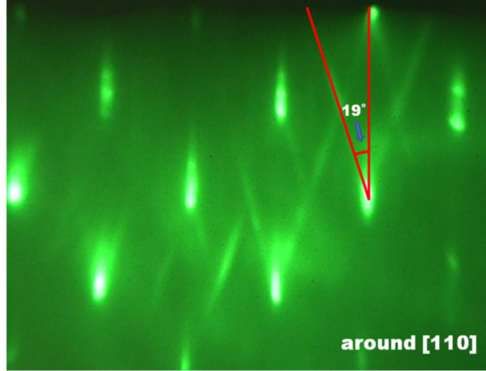

FIG. 3. RHEED pattern formed from the surface with the Sn-rich island array on the pedestals. The facet angle, at which the pedestal is faceted, corresponds to the face orientation (311).

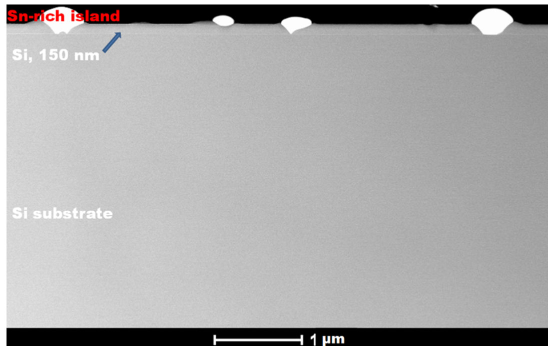

FIG. 5. Cross-sectional TEM image from the sample containing the SiSn island array with the Si pedestals. It shows the absence of dislocations in the structure. The Si thickness of 15 nm corresponds to the upper Si layer deposited on the surface with the Sn island array.

© Author(s) 2020

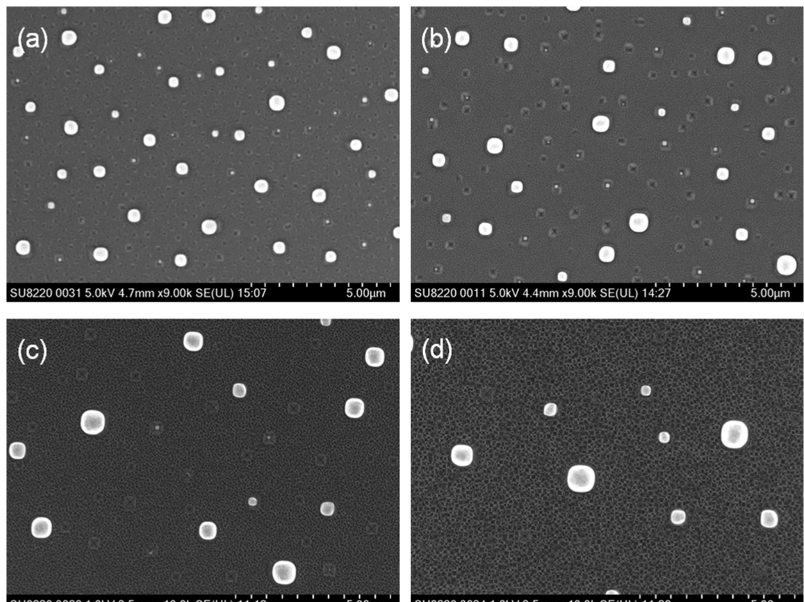

FIG. 6. SEM images of the surface for samples A1 (a), A2 (b), A3 (c), A4 (d) (see Table I).

at the temperature exceeding the Sn melting temperature. Returning to the issue on the appearance of pits, we assume that pits are formed during the Si deposition in the presence of a Sn island array. As the Si deposition temperature exceeds Sn melting temperature, the initial Sn islands are liquid drops. As a result of the tin-rich island merging, part of the islands disappears, forming a pedestal with a pit in the center or near it. Silicon builds in, primarily, close to the base, thus forming pedestals. Moreover, a solid SiSn solution should form at the Si-Sn border. The element composition of the obtained structures with the island array on the pedestals with the methods of EDX and XPS is described below. The interisland surface on the pedestals and large faceted pits is cellular. The samples with a cellular surface structure can serve as a nanostructured substrate. The rise of the Si deposition temperature leads to a density decrease in the islands with pedestals (Fig. 6). The Si growth temperature changes from 450 up to 600 °C. The cells become more distinct with a temperature increase, but they can increase in their size. The element composition was analyzed by the EDX spectroscopy built in the SEM-system and XPS spectroscopy. The element composition map obtained by the method of EDX spectroscopy is presented.[17] One can conclude that the pedestal is silicon-rich based on the analysis by mapping the element distribution. The islands on the pedestals are tin-rich. A preliminary analysis of the chemical composition in the plan-view geometry (top view) shows the island tin content to 90%. The study of the chemical state of materials for the Sn island array and the Sn-rich droplet with the pedestal was performed by X-Ray photoelectron spectroscopy as well. The photoelectron spectra of the $Sn3d_{5/2}$ and Si 2p regions for the sample with the Sn islands are shown in Fig. 7. The Sn island array was obtained after the 5 nm thick Sn film deposition and annealing at the temperatures of 100 °C and 400 °C, respectively. The $Sn3d_{5/2}$ region decomposition shows the presence of peaks, corresponding to different Sn oxidation degrees of 0 (metal), +2 (SnO), +4 (SnO_2). The binding energy value for Sn^0 is 484.8 eV. Moreover, the photoelectron spectra of the wet-etched sample S4 (Table II) were measured and are shown in Fig. 8. The wet etching realized for 2 min in the 1:2 HNO_3:HCl mixture was carried out before X-Ray photoelectron spectroscopy. The analysis of $Sn3d_{5/2}$ photoelectron spectra for the fresh sample [Fig. 8(a)] and the sample after the Ar^+ ion etching for 20 min [Fig. 8(b)] was performed. The sharp Sn^0 line is observed after the Ar^+ ion etching and corresponds to a value of about 485.1 eV. The difference between the Sn^0 binding energy for

TABLE I. Sample description.

Number of the sample	Sn thickness (nm)	Sn growth temperature (°C)	Sn annealing temperature (°C)	Si thickness (nm)	Si growth temperature (°C)
A1	5	300	...	100	450
A2	5	300	...	100	500
A3	5	300	...	100	550
A4	5	300	...	100	600

© Author(s) 2020

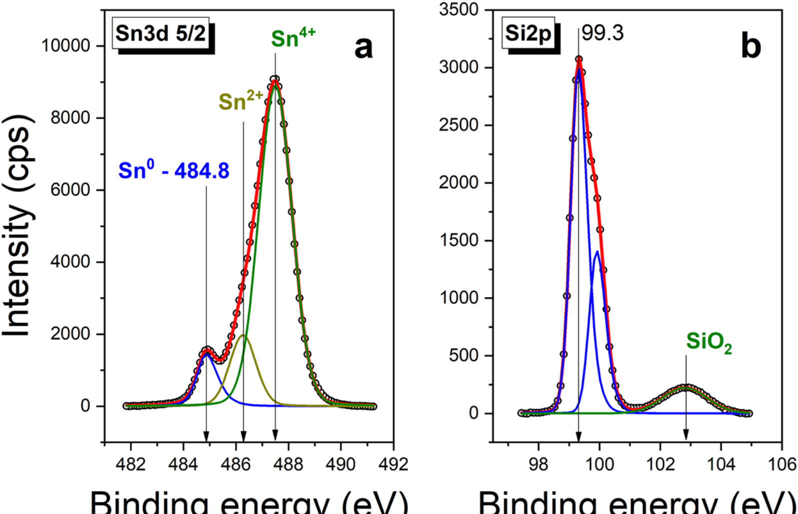

FIG. 7. Photoelectron spectra of $Sn3d_{5/2}$ (a) and Si 2p (b) regions for the sample with Sn islands. The Sn island array was obtained after the 5 nm thick Sn film deposition and annealing at the temperatures of 100 °C and 400 °C, respectively.

TABLE II. Sample description.

Number of the sample	Sn thickness (nm)	Sn growth temperature (°C)	Sn annealing temperature (°C)	Si thickness (nm)	Si growth temperature (°C)
S1	5	100	400	100	350
S2	5	100	375	100	350
S3	5	Room temperature	400	100	400
S4	20	Room temperature	400↑450	150	400
S5	20	Room temperature	350	100	350
S6	20	100	350	100	350

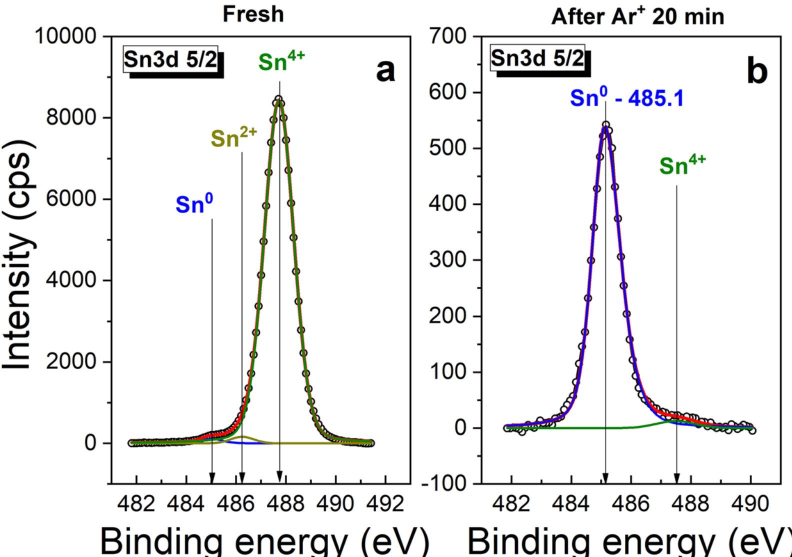

FIG. 8. Photoelectron spectra of the $Sn3d_{5/2}$ regions for wet-etched sample S4: (a) the photoelectron spectrum from the fresh sample and (b) the photoelectron spectrum from the sample after the Ar ion etching for 20 min.

© Author(s) 2020

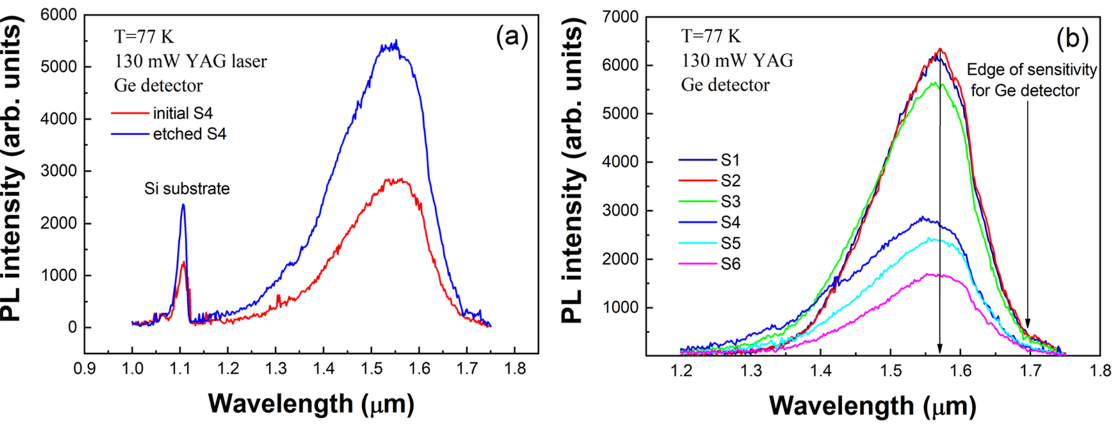

FIG. 9. Photoluminescence spectra: (a) from sample S4 before and after wet etching and (b) from samples S1, S2, S3, S4, S5, and S6 (see Table II).

the sample with the Sn islands (Fig. 7) and the wet-etched sample S4 after the Ar^+ ion etching [Fig. 8(b)] equals 0.3 eV. This may be the evidence in favor of the SiSn solid solution formation. The similar shift effects were registered in the bimetallic alloys.[18,19]

The optical properties of the tin-rich island arrays on the pedestals were studied with the methods of photoluminescence spectroscopy. The photoluminescence spectra for sample S4, before and after etching, are shown in Fig. 9. As it turned out, the photoluminescence signal grows for the postetched sample. Therefore, photoluminescence is, definitely, not connected with tin-rich islands. The photoluminescence spectra for the series of the samples described in Table II are presented in Fig. 9(b). Two sets of the spectra, almost two times different in their photoluminescence intensity, are observed. The samples which differ in the initial tin thickness (5 and 20 nm) correspond to the above sets of the spectra. The solid SiSn solution, which is formed at the tin-rich (to 90% Sn) island-silicon pedestal, can mainly contribute to the photoluminescence. This assumption is proved by the band diagram calculation for the SiSn/Si heterotransition and also by the X-ray photoelectron spectroscopy data. The calculation was carried out using the approach of model solid theory.[20] A Sn content of about 15% corresponds to the transition close to the photoluminescence maximum (wavelength of about 1.55 μm). This value significantly exceeds the equilibrium solubility limit of tin in silicon and, probably, can be reached in the structures we obtained (at the tin-rich island–silicon pedestal border).

IV. CONCLUSION

The work aimed at studying the morphology and structure of thin tin films, as well as creating a tin island array on the Si surface during the Sn deposition by molecular beam epitaxy at room temperature and 100 °C with a subsequent annealing or the Sn growth at 300 °C. The growth and annealing of tin films for thicknesses from 0 to 20 nm were controlled by reflection high energy electron diffraction. The appearance of tin islands was accompanied by the occurrence of three-dimensional reflexes in the diffraction pattern. A Sn island array was used further to study the growth of nanostructures in the process of Si deposition on the surface with Sn islands. It was established that, during the growth on the vapor-liquid-crystal mechanism, tin-rich islands are formed on faceted pedestals. A nanostructured cellular surface is formed between islands on pedestals. An increase in the Si deposition temperature leads to a decrease in the density of islands and the appearance of a distinct surface structure shaped as nanosized faceted cells, which have the shape of a reverse pyramid. The analysis of the elemental composition of the obtained nanostructures was performed by the methods of energy dispersive X-ray spectroscopy and photoelectron spectroscopy. It was shown that tin-rich islands can contain up to 90% of tin, whereas the pedestal consists of silicon. In addition, based on the results obtained by photoelectron spectroscopy, it was concluded that a SiSn solid solution layer is formed on the tin-rich island-silicon pedestal border. The transmission electron microscopy data demonstrated a distinct crystal structure of tin-rich islands and silicon pedestals, as well as the absence of dislocations in the structures with island arrays on pedestals. The silicon pedestal facet orientation was determined by reflection high energy electron diffraction and transmission electron microscopy. The facet tilt angle is 19° and corresponds to the (311) plane. The optical properties of structures, including tin-rich island arrays on silicon pedestals, were studied by the photoluminescence method. The photoluminescence signal was obtained at the temperature of 77 K and was observed in the range of 1.3–1.7 μm with the photoluminescence maximum close to the wavelength of 1.55 μm. Since the structures including island arrays on pedestals do not contain dislocations, it can be concluded that the photoluminescence signal is observed from the solid solution layer.

ACKNOWLEDGMENTS

This work was supported by the Russian Science Foundation (RSF), Grant No. 18-72-00090 (Figs. 2, 3, 6, and 9 obtained within the project), and by the Russian Foundation for Basic Research, Grant No. 18-32-20064 (the Sn film growth was investigated in the range of thicknesses from 0 to 20 nm, Fig. 1), Grant No. 18-42-540018 (Fig. 5), and Grant No. 18-52-41006 (Figs. 7 and 8). HRTEM and SEM study was carried out with the support of RSF (Grant No. 19-72-30023) and using the equipment of CCP "Nanostructures."

© Author(s) 2020

REFERENCES

[1] T. R. Harris, M. Y. Ryu, Y. K. Yeo, B. Wang, C. L. Senaratne, and J. Kouvetakis, "Direct bandgap cross-over point of $Ge_{1-y}Sn_y$ grown on Si estimated through temperature-dependent photoluminescence studies," J. Appl. Phys. **120**, 085706 (2016).
[2] C. L. Senaratne, P. M. Wallace, J. D. Gallagher, P. E. Sims, J. Kouvetakis, and J. Menendez, "Direct gap $Ge_{1-y}Sn_y$ alloys: Fabrication and design of mid-IR photodiodes," J. Appl. Phys. **120**, 025701 (2016).
[3] J. D. Gallagher, C. Xu, C. L. Senaratne, T. Aoki, P. M. Wallace, and J. Kouvetakis, "$Ge_{1-x-y}Si_xSn_y$ light emitting diodes on silicon for mid-infrared photonic applications," J. Appl. Phys. **118**, 135701 (2015).
[4] N. von den Driesch, D. Stange, S. Wirths, D. Rainko, I. Povstugar, A. Savenko, U. Breuer, R. Geiger, H. Sigg, Z. Ikonic, J. M. Hartmann, D. Grützmacher, S. Mantl, and D. Buca, "SiGeSn ternaries for efficient group IV heterostructure light emitters," Small **13**, 1603321 (2017).
[5] S. Wirths, R. Geiger, N. von den Driesch, G. Mussler, T. Stoica, S. Mantl, Z. Ikonic, M. Luysberg, S. Chiussi, J. M. Hartman, H. Sigg, J. Faist, D. Buca, and D. Grutzmacher, "Lasing in direct-bandgap GeSn alloy grown on Si," Nat. Photonics **9**, 88 (2015).
[6] B.-J. Huang, C.-Y. Chang, Y.-D. Hsieh, R. A. Soref, G. Sun, H.-H. Cheng, and G.-E. Chang, "Electrically injected GeSn vertical-cavity surface emitters on silicon-on-insulator platforms," ACS Photonics **6**, 1931–1938 (2019).
[7] N. von den Driesch, D. Stange, D. Rainko, I. Povstugar, P. Zaumseil, G. Capellini, T. Schröder, T. Denneulin, Z. Ikonic, J. M. Hartmann, H. Sigg, S. Mantl, D. Grützmacher, and D. Buca, "Advanced GeSn/SiGeSn group IV heterostructure lasers," Adv. Sci. **5**, 1700955 (2018).
[8] T. Yamaha, S. Shibayama, T. Asano, K. Kato, M. Sakashita, W. Takeuchi, O. Nakatsuka, and S. Zaima, "Experimental observation of type-I energy band alignment in lattice-matched $Ge_{1-x-y}Si_xSn_y$/Ge heterostructures," Appl. Phys. Lett. **108**, 061909 (2016).
[9] A. P. Alivisatos, "Semiconductor clusters, nanocrystals, and quantum dots," Science **271**, 933–937 (1996).
[10] C. Qi, G. Goncher, R. Solanki, and J. Jordan, "SiGe nanowire growth and characterization," Nanotechnology **18**, 075302 (2007).
[11] U. Givan, M. Kwiat, and F. Patolsky, "The influence of doping on the chemical composition, morphology and electrical properties of $Si_{(1-x)}Ge_x$ nanowires," J. Phys. Chem. C **114**, 4331–4335 (2010).
[12] J. Xiang, A. Vidan, M. Tinkham, R. M. Westervelt, and C. M. Lieber, "Ge/Si nanowire mesoscopic Josephson junctions," Nat. Nanotechnol. **1**, 208–213 (2006).
[13] M. S. Seifner, A. Dijkstra, J. Bernardi, A. Steiger-Thirsfeld, M. Sistani, A. Lugstein, J. E. M. Haverkort, and S. Barth, "Epitaxial $Ge_{0.81}Sn_{0.19}$ nanowires for nanoscale mid-infrared emitters," ACS Nano **13**, 8047–8054 (2019).
[14] F. Todescato, I. Fortunati, A. Minotto, R. Signorini, J. Jasieniak, and R. Bozio, "Engineering of semiconductor nanocrystals for light emitting applications," Materials **9**, 672 (2016).
[15] R. J. A. Esteves, S. Hafiz, D. O. Demchenko, Ü. Özgür, and I. U. Arachchige, "Ultra-small $Ge_{1-x}Sn_x$ quantum dots with visible photoluminescence," Chem. Commun. **52**, 11665–11668 (2016).
[16] S. A. Hafiz, R. J. A. Esteves, D. O. Demchenko, I. U. Arachchige, and Ü. Özgür, "Energy gap tuning and carrier dynamics in colloidal $Ge_{1-x}Sn_x$ quantum dots," J. Phys. Chem. Lett. **7**, 3295–3301 (2016).
[17] A. I. Nikiforov, V. A. Timofeev, V. I. Mashanov, T. A. Gavrilova, and D. V. Gulyaev, "Elastically stressed pseudomorphic SiSn island array formation with a pedestal on the Si(100) substrate using Sn as a growth catalyst," J. Cryst. Growth **518**, 103–107 (2019).
[18] A. V. Bukhtiyarov, I. P. Prosvirin, and V. I. Bukhtiyarov, "XPS/STM study of model bimetallic Pd-Au/HOPG catalysts," Appl. Surf. Sci. **367**, 214–221 (2016).
[19] C. W. Yi, K. Luo, T. Wei, and D. W. Goodman, "The composition and structure of Pd-Au surfaces," J. Phys. Chem. B **109**, 18535–18540 (2005).
[20] V. A. Timofeev, A. I. Nikiforov, A. R. Tuktamyshev, V. I. Mashanov, I. D. Loshkarev, A. A. Bloshkin, and A. K. Gutakovskii, "Pseudomorphic GeSiSn, SiSn and Ge layers in strained heterostructures," Nanotechnology **29**, 154002 (2018).

© Author(s) 2020